Journal of Solid State Chemistry 182 (2009) 1061–1069

Contents lists available at ScienceDirect

Journal of Solid State Chemistry

journal homepage: www.elsevier.com/locate/jssc

Sonochemical fabrication of fluorinated mesoporous titanium dioxide microspheres

Changlin Yu [a,b], Jimmy C. Yu [b,*], Mui Chan [b]

[a] School of Materials and Chemical Engineering, Jiangxi University of Science and Technology, 86 Hongqi Road, Ganzhou 341000, Jiangxi, PR China
[b] Department of Chemistry, The Center of Novel Functional Molecules and Environmental Science Programme, The Chinese University of Hong Kong, Shatin, New Territories, Hong Kong, China

ARTICLE INFO

Article history:
Received 25 October 2008
Received in revised form
10 January 2009
Accepted 26 January 2009
Available online 5 February 2009

Keywords:
TiO_2 microspheres
Ultrasonic irradiation
Fluorination
Hydrothermal treatment
Photocatalysis

ABSTRACT

A sonochemical–hydrothermal method for preparing fluorinated mesoporous TiO_2 microspheres was developed. Formation of mesoporous TiO_2 and doping of fluorine was achieved by sonication and then hydrothermal treatment of a solution containing titanium isopropoxide, template, and sodium fluoride. The as-synthesized TiO_2 microspheres were characterized by X-ray diffraction (XRD), Fourier translation infrared spectroscopy (FT-IR), X-ray photoelectron spectroscopy (XPS), scanning electron microscopy (SEM), transmission electron microscopy (TEM), energy-dispersive X-ray (EDX) spectroscopy, photoluminescence spectroscopy (PL), and BET surface areas. The P123 template was removed completely during the hydrothermal and washing steps, which was different from the conventional calcination treatment. The as- synthesized TiO_2 microspheres had good crystallinity and high stability. Results from the photocatalytic degradation of methylene blue (MB) showed that fluorination could remarkably improve the photocatalytic activity of titanium dioxide.

1. Introduction

Semiconductor photocatalysts have attracted much attention in the past decades owing to their applications to environmental purification and solar energy conversion [1–4]. Among photocatalysts, TiO_2 has received the most attention as a photocatalytic material because of its superior photocatalytic activity, chemical stability, low cost, and nontoxicity [5–8].

It is well known that the first step of a heterogeneous photocatalytic process, generation of the electron (e^-)–hole (h^+) pairs, is initiated upon irradiation of photons with energy greater than or equal to the band gap energy of the photocatalyst. The photogenerated electrons and holes can either recombine in the bulk to produce thermal energy, or migrate to the surface and react with adsorbed species at the surface. Obviously, electron and hole recombination is detrimental to the efficiency of a semiconductor photocatalyst.TiO_2-based photocatalysts doped with anions (e.g. C, N, S, F) [9–13] have been widely investigated in order to reduce the recombination of photogenerated electrons and holes or extend its light absorption into the visible region. Among these, the fluorine-doping or surface fluorination of TiO_2 has been found to be a most effective method to promote the activity of TiO_2 [14–20]. Our previous research showed that an appropriate amount of F-doping would not only slow down the radiative recombination process of photogenerated electrons and holes in TiO_2, but also improve the crystallinity of anatase [13]. Minero et al. [14] reported that the photocatalytic oxidation (PCO) of phenol was enhanced with F–TiO_2 and proposed that the fluorinated surface favored the generation of free OH radicals (not surface-bound ···OH), which were responsible for the enhanced oxidation. Park et al. [18] have recently found that F–TiO_2 could enhance the remote photocatalytic oxidation at the air/catalyst interface by facilitating the desorption of OH radicals under UV irradiation.

Mesoporous titania in the form of films, spheres and hollow structures hold much promise as heterogeneous photocatalysts due to high specific surface area, excellent transport behavior, and large porosity. To achieve a high surface area and meso or microporous structure, titania has been fabricated using different organic templating procedures [21,22]. However, the preparation of mesoporous titanium dioxide with high surface area, well ordered structure, uniform pore size and thermal stability has still remained unsolved [23–26]. Experimental drawbacks are mainly associated with the calcination step, which is used for the removal of the template. During calcination the ordered structure of the mesoporous TiO_2 collapses and/or the surface area decreases significantly [27].

Sonochemical processing has been proven to be a useful technique to synthesize novel materials with unusual properties [28–31]. The chemical effects of ultrasound irradiation arise from

* Corresponding author. Fax: +852 2603 5057.
E-mail address: jimyu@cuhk.edu.hk (J.C. Yu).

0022-4596/$ - see front matter © 2009 Elsevier Inc. All rights reserved.
doi:10.1016/j.jssc.2009.01.033

acoustic cavitation. That is, the formation, growth and collapse of bubbles in a liquid. The extremely high temperatures (~5000 °C), pressures (>20 Mpa), and cooling rates ($>10^{9\circ}\,s^{-1}$) attained during cavitation collapse lead to many unique properties in the irradiated solution, and these extreme conditions have been exploited to decompose the metal–carbonyl bonds and generate nanoscale metals [32], metal carbides [33], metal oxides and sulfides[34]and nanocomposites [35].

In this study, we describe a facile and efficient approach for the fabrication of fluorinated mesoporous TiO_2 microspheres by combining ultrasound irradiation with hydrothermal treatment. The obtained fluorinated TiO_2 microspheres have high anatase crystallinity, high stability and greatly enhanced photocatalytic activity. This method does not require the traditional calcination treatment to remove the template. To the best of our knowledge, this is the first report on the fluorinated TiO_2 microspheres by a sonochemical approach.

2. Experimental

2.1. Synthesis

The method of synthesis was according to our previous method with some modifications [36]. In a typical synthesis, 9.6 g titanium isopropoxide (TIP), 3.2 g P123, and 0.96 g glacial acetic acid were dissolved in 30 mL absolute ethanol. After stirring for 40 min, the resulting solution was added dropwise to 120 mL deionised (DI) water under sonication in air. Ultrasound irradiation was accomplished with a high-intensity ultrasonic probe (Xinzhi Co., Xinzhi, China; 2 cm diameter; Ti-horn, 20 kHz, 250 W/cm^2) immersed directly in the reaction solution. During the whole process, the sonication cell was water-cooled to avoid overheating. After sonicating for 2 h (3 s on, 1 s off), 1.1 g NaF was added to the slurry and further sonication for 1 h. The slurry was placed in a Teflon-lined stainless steel autoclave maintained at 180 °C for 10 h. The powders were collected by centrifugation, washed two times with DI water and one time with ethanol, dried in an oven at 100 °C. The color of the fluorinated sample was shallow red, while the prepared pure titanium dioxide was white.

2.2. Characterization

Fourier translation infrared spectroscopy (FT-IR) spectrum was recorded with a Nicolet 560 FTIR spectrometer (USA). Samples were pressed by a KBr disk preparation apparatus.

The BET surface areas of the sample were obtained from N_2 adsorption/desorption isotherms determined at liquid nitrogen temperature on an automatic analyzer (Micromeritics, ASAP 2010). The samples were outgassed for 2 h under vacuum at 180° prior to adsorption.

X-ray diffraction (XRD) patterns, obtained on a Bruker D8 Advance X-ray diffractometer using Cu$K\alpha$ radiation at a scan rate of $0.05^\circ(2\theta)\,s^{-1}$, were used to identify the phase constitution in samples and their crystallite size. The accelerating voltage and the applied current were 40 kV and 40 mA, respectively.

The general morphology of the products was characterized by scanning electron microscopy (SEM, LEO, 1450VP). The products were conductively coated with gold by sputtering for 30 s to minimize charging effects under SEM imaging conditions. Transmission electron microscopy (TEM) images were recorded on a CM-120 microscope (Philips, 120 kV) coupled with an energy-dispersive X-ray (EDX, Oxford Instrument) spectrometer. Samples were deposited on thin amorphous carbon films supported by copper grids from ultrasonically processed ethanol solutions of the products.

The samples were also analyzed by X-ray photoelectron spectroscopy on a PHI Quantum 2000 XPS System with a monochromatic AlKa source and a charge neutralizer. All the binding energies were referenced to the C1*s* peak at 284.8 eV of the surface adventitious carbon.

To investigate the recombination and lifespan of photogenerated electrons/holes in the photocatalysts, the photoluminescence (PL) emission spectra of the samples were recorded. A 280 nm He–Cd laser was used as an excitation light source. The emission from the sample was measured by a spectrometer (Spex 500M, USA) equipped with a photon counter (SR400, USA).

2.3. Photocatalytic activity measurement

The photocatalytic activities of the prepared pure TiO_2 and fluorinated TiO_2 were determined by measuring the degradation of methylene blue (MB) in an aqueous solution under UV light irradiation. A 365 nm UV lamp (Cole-Parmer Instrument Co.) was used as light source. The photocatalyst (0.05 g) was suspended in an 80 mL aqueous solution of $C_0 = 0.008$ g/L. Before the lamp was turn on, the suspension was stirred in the dark for 40 min. The suspension was vigorously stirred with the photoreactor during the process and the temperature of suspension was maintained at $22\pm2^\circ$ by circulation of water through an external cooling coil. At given intervals of illumination, the sample of suspension was taken out and centrifuged. The clear upper layer solution was analyzed by a Milton Roy Spectronic 3000 Array spectrophotometer (NY, USA). The dye concentration was measured at $\lambda = 663$ nm, the maximum absorption wavelength for MB.

3. Results and discussion

3.1. SEM and TEM analysis

Fig. 1 shows the typical SEM images of the as-synthesized TiO_2 product. The overall morphology of the product is shown in Figs. 1a and b. It is observed that both the pure TiO_2 and fluorinated TiO_2 are composed of a large quantity of relatively uniform microspheres with an average diameter of about 1.5 μm. Figs. 1c and d show the morphology of the product at higher magnification, indicating these TiO_2 spheres with a perfectly spherical shape and a rough surface. Some small spherical crystals can be observed over the rough surface, indicating that the large spheres were the product of the small spherical crystals aggregation. In order to test the stability of these microspheres, a calcination treatment (at 400° for 1 h) was carried out. Figs. 1e and f show the morphology of the product after calcination. The size of the microspheres became smaller after calcination, but the morphology of the products were almost integral.

The morphology and composition of the as-prepared samples were further investigated with TEM and EDX analyses. TEM observations, Figs. 2a and b, show that the average crystallite size is about 9–10 nm. Fig. 3 is an EDX spectrum of the fluorinated TiO_2 spheres the showing elements of C, O F and Cu (the Cu peaks come from the supporting copper grid). These results confirm that the F was introduced into TiO_2 spheres.

3.2. BET analysis

Fig. 4 shows nitrogen adsorption–desorption isotherms (inset) and pore size distribution plots for the as-synthesized TiO_2 microspheres. Both samples show a type-IV isotherm, which is representative of mesoporous solids. The specific surface area of

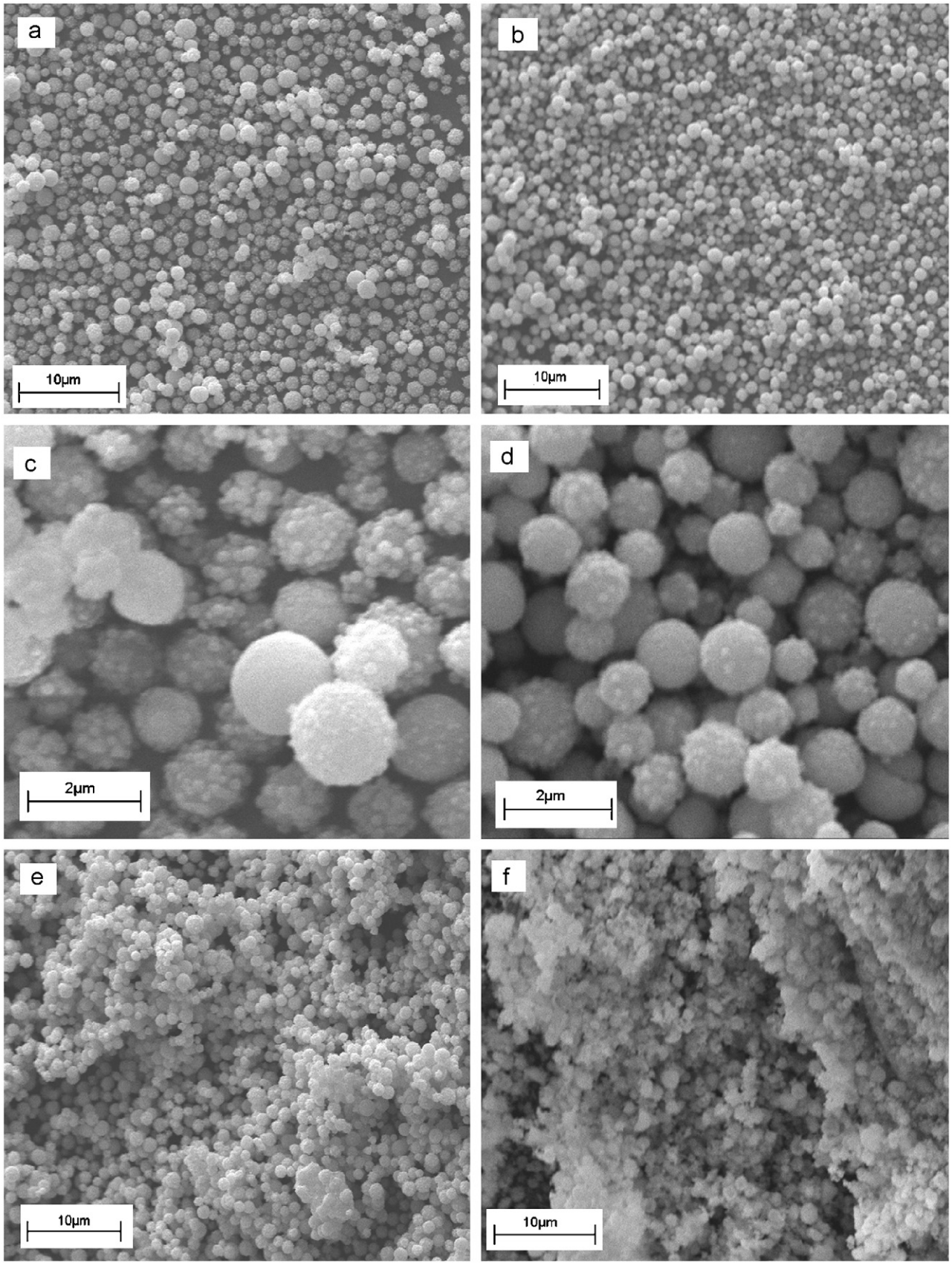

Fig. 1. SEM images of the pure and fluorinated TiO_2 microspheres. (a) and (b) for as-synthesized pure and fluorinated TiO_2 microspheres; (c) and (d) higher magnification images of as-synthesized pure and fluorinated TiO_2 microspheres; (e) and (f) for calcined pure and fluorinated TiO_2 microspheres.

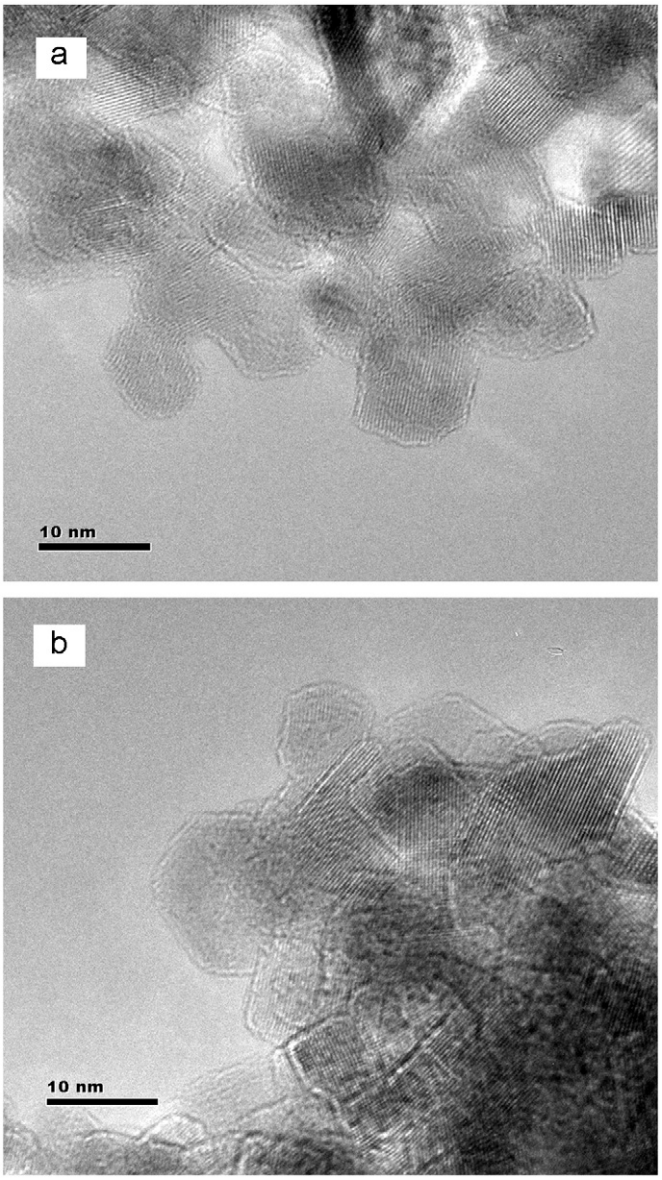

Fig. 2. TEM images of the as-synthesized pure (a) and fluorinated (b) TiO_2 microspheres.

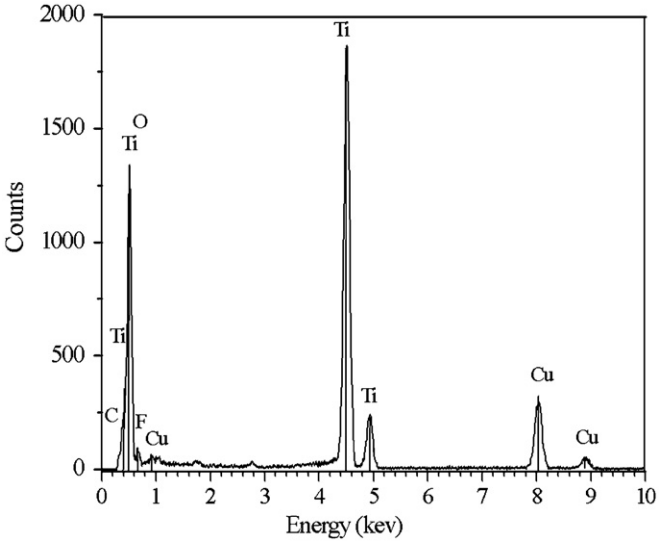

Fig. 3. EDX spectrum of the as-synthesized fluorinated TiO_2 microspheres.

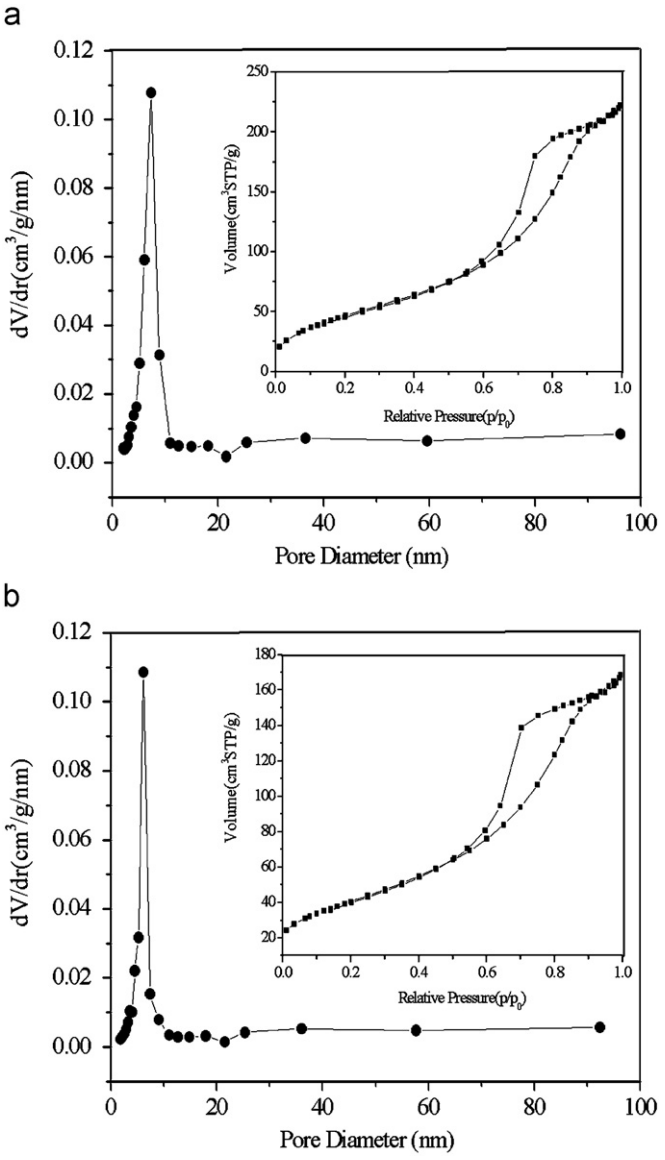

Fig. 4. (a, b) N_2-sorption isotherms (inset) and corresponding pore-size distribution curves for as-synthesized pure TiO_2 and fluorinated TiO_2 microspheres, respectively.

the pure TiO_2 is 180 m^2/g using the Brunauer–Emmett–Teller (BET) method. The pore diameter of the pure TiO_2 is 6.4 nm (estimated using the desorption branch of the isotherm) with very narrow pore size distribution. The fluorinated TiO_2 possesses average pore diameter of 7.2 nm and have relatively low specific surface area (160 m^2/g). The pore volume is virtually identical for pure (0.35 cm^3/g) and fluorinated TiO_2 (0.34 cm^3/g). The influence of calcination treatment on the structure of products is summarized in Table 1. The calcination treatment caused only a small decrease in both BET surface area and pore volume, but resulting in an increase in pore size. These results were very different from the usual template removal by calcinations, in which a huge loss of surface area would be expected.

3.3. IR analysis

One of the major problems in the synthesis of mesoporous TiO_2 is associated with the removal of the template, which usually causes undesirable damages in the delicate mesostructure. Calcination or extraction is often required for the removal of

Table 1
BET surface areas, pore volume, pore size and crystalline size in the samples.

Sample	S_{BET}[a] (m^2/g)	Pore volume[b] (cm^3/g)	Pore size[c] (nm)	Crystalline size[d] (nm)
a1	180	0.35	6.4	9
a2	158	0.34	7.2	13
b1	148	0.27	6.1	10
b2	131	0.25	8.4	11

a1: pure TiO_2 microspheres; a2: calcined pure TiO_2 microspheres, b1: fluorinated TiO_2 microspheres; b2: calcined fluorinated TiO_2 microspheres.

[a] BET surface area calculated from the linear part of the BET plot ($P/P_0 = 0.05$–0.3).

[b] Total pore volume, taken from the volume of N_2 adsorbed at $P/P_0 = 0.995$.

[c] Average pore diameter, estimated using the adsorption branch of the isotherm and the Barrett–Joyner–Halenda formula.

[d] Calculated from X-ray line broadening analysis by Scherrer formula from XRD result from anatase phase.

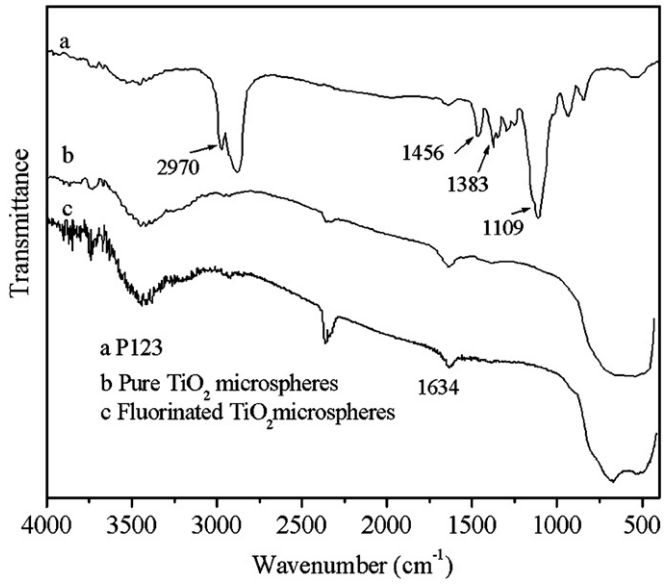

Fig. 5. FT-IR spectrums of P123 removal study.

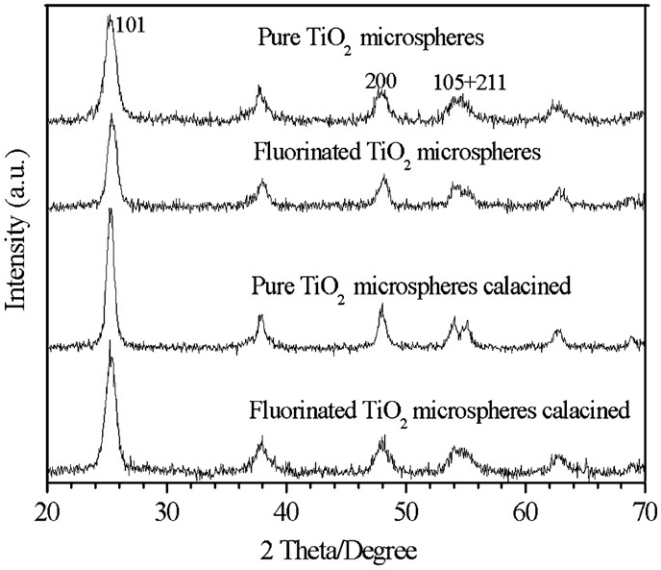

Fig. 6. XRD patterns of the pure TiO_2 and fluorinated TiO_2 microspheres.

3.4. XRD analysis

XRD patterns were used to determine the crystalline forms and crystallinity of as-synthesized and calcined TiO_2 microspheres. As shown in Fig. 6, the four XRD patterns exhibit the same diffraction peaks at 2θ of 25.3°, 38.2°, 48.1°, 53.5° and 55.6°. These peaks are attributed to anatase–TiO_2 (JCPDF84-1285), as indexed in Fig. 6. These as-synthesized TiO_2 microspheres have good crystallinity. The average crystallite sizes of anatase were determined according to the Scherrer equation using the fwhm data of each phase after correcting the instrumental broadening [37,38]. The crystalline size is about 9 and 10 nm for pure TiO_2 and fluorinated TiO_2 microspheres, respectively, which is accordance with the TEM test. The fluorination has no obvious effects on the crystal structure of TiO_2. A slight increase in the intensity of the peak (101) was observed after the calcination treatment. The crystallite size over pure TiO_2 microspheres increased from 9 to 13 nm, as indicated in Table 1. But, it is not the case for fluorinated TiO_2 microspheres. No obvious increase in the crystallite size over the fluorinated TiO_2 was observed.

the structure directing templates. One of the attractive features of our method is that no calcination or extraction treatment is needed for template removal. Fig. 5 shows the FTIR spectrum of a fluorinated TiO_2 sample. All peaks related to P123 are absent. These include the stretching vibration ($-CH_3$, $-CH_2-$) in the range 3000–2800 cm^{-1}, bending vibration (C–H) at 1456 and 1384 cm^{-1}, and stretching vibration of C–O–C. In the hydrothermal process, the inorganic framework is transformed to mesostructured TiO_2 by polycondensation over the surface of the amphiphilic micelle. P123 is a nonionic surfactant. The interactions between the triblock copolymer template and inorganic framework are weak hydrogen bonds. During the course of hydrothermal process, the size of micelles in water increases gradually. When the pores of inorganic framework shrink to a certain extent, the amphiphilic molecules are expelled from the pore to form the larger micelles in water. At the same time, water molecules enter into the pores of the inorganic frame by capillary action. After hydrothermal treatment, yellow P123 aggregates are left in the suspension. These aggregates are removed easily in the washing process.

3.5. X-ray photoelectron spectroscopy (XPS) analysis

The elemental composition of fluorinated TiO_2 microspheres was further determined by XPS. Fig. 7a shows that the prepared fluorinated TiO_2 microspheres consist of Ti, O, C and F. The C element was mainly ascribed to the adventitious hydrocarbon from XPS itself [39]. Fig. 7b shows the high-resolution XPS spectra of F1*s*. An unsymmetrical F1*s* peak was observed. This means that two chemical forms of F-atoms might exist in fluorinated TiO_2 microspheres. Therefore, the F1*s* peak of each sample was deconvoluted into two peaks with Gaussian distributions. Peak 1 located at 685.3 eV was attributed to the F atoms in $TiOF_2$ [40,41]. The peak 2 located at 687.0 eV could attributed to the substitutional F-atoms in TiO_2, that is, the substitutional F atoms that occupied oxygen sites in the TiO_2 crystal lattice, and the position of this peak was close to the value previous reported by our group for the substitutional F atoms in TiO_2 [13]. The XPS spectra of the O1*s* region are shown in Fig. 7c. The O1*s* region could be fitted by two peaks at 531.3 eV and 532.1 eV, corresponding to the Ti–O bond in TiO_2, hydroxyl groups on the surface. Fig. 7d shows that

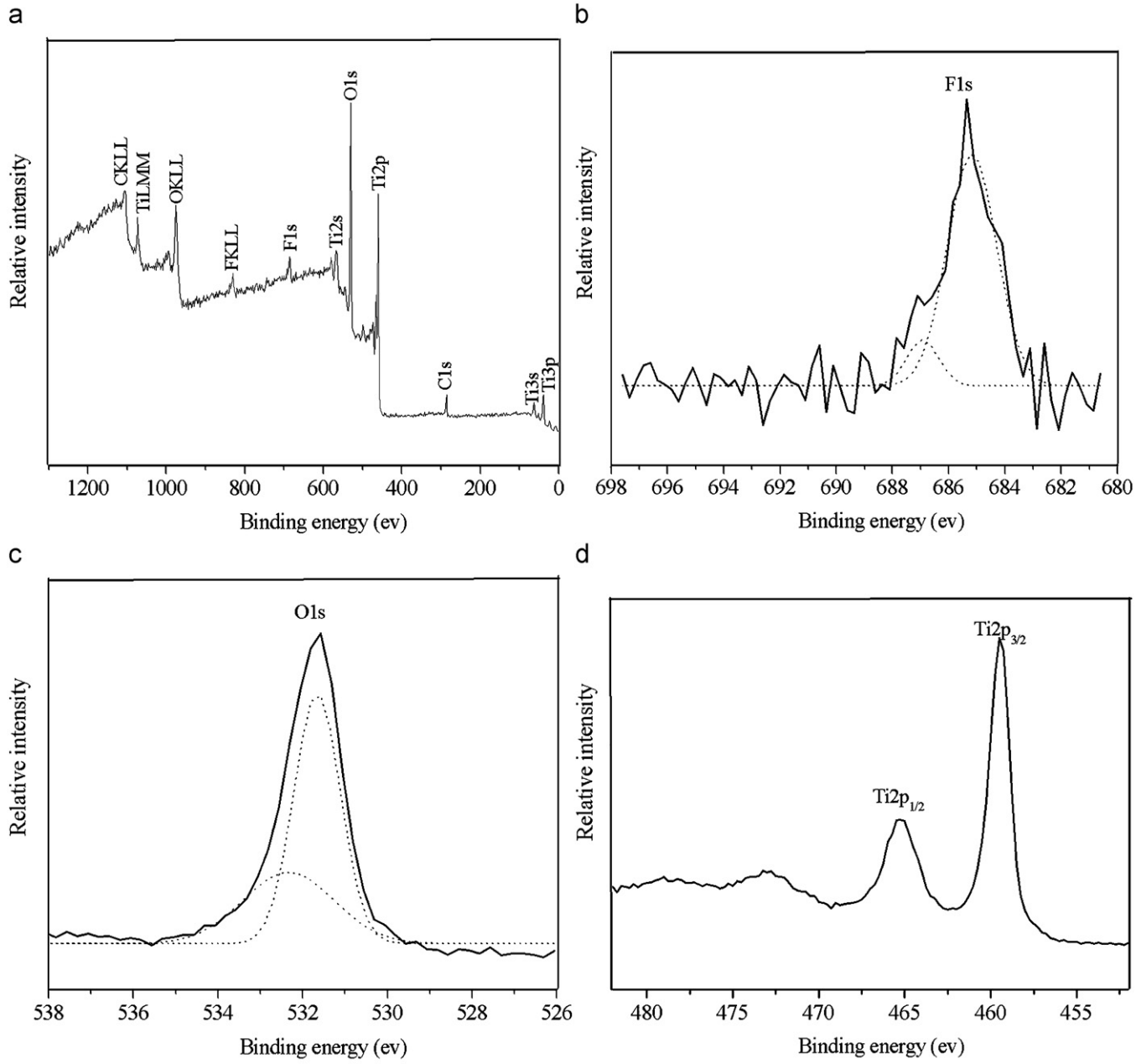

Fig. 7. The survey spectrum (a), F1*s* XPS spectra (b), O1*s* XPS spectra (c), and Ti2*p* XPS spectra (d) of fluorinated TiO_2 microspheres.

Ti2*p*3/2 in TiO_2 at 459.5 eV, indicating an octahedral coordination for the environment of Ti ions.

3.6. Mechanism for the formation of fluorinated TiO_2 microspheres

A possible mechanism for the formation of fluorinated TiO_2 microspheres was suggested as Fig. 8. At the beginning, titanium isopropoxide and P123 are dissolved in ethanol to form a homogeneous solution. When this solution was added dropwise to DI water under sonication, partially hydrolyzed alkoxides (titanium oxo clusters) sol particles were formed by the slow hydrolysis and condensation of acetic acid modified TIP. These kinds of precursors have many hydroxyl groups (−OH), which can interact with the blocks of triblock copolymer templates via hydrogen bonds, forming mesostructured hybrid inorganic/organic precursory particles [42]. These hydrophobic, partially hydrolyzed particles can be emulsified as droplets in the reaction mixture and stabilized by a surfactant. At the same time, a high-speed collision driven by high intensity ultrasound irradiation can generate localized high temperature regions. This can enhance the condensation reactions among hydroxyl groups on adjacent mesoporous spherical particles, to produce the agglomerates of spherical particles [29,36,43]. In a control experiment without sonication, no such uniform microspheres can be obtained even under vigorous stirring. When the NaF is added, the fluorination reaction takes place by a simple ligand exchange between surface hydroxyl groups on TiO_2 and fluoride ions in water as Eq. (1):

$$\equiv \mathrm{Ti{-}OH} + \mathrm{F^-} \rightarrow \equiv \mathrm{Ti{-}F} + \mathrm{OH^-} \quad (1)$$

Sonication also speeds up the fluorination reaction resulting in a color change of the slurry from white to gray. During the hydrothermal process, the titanium sol particles are further hydrolyzed and crystallized to the highly crystalline anatase

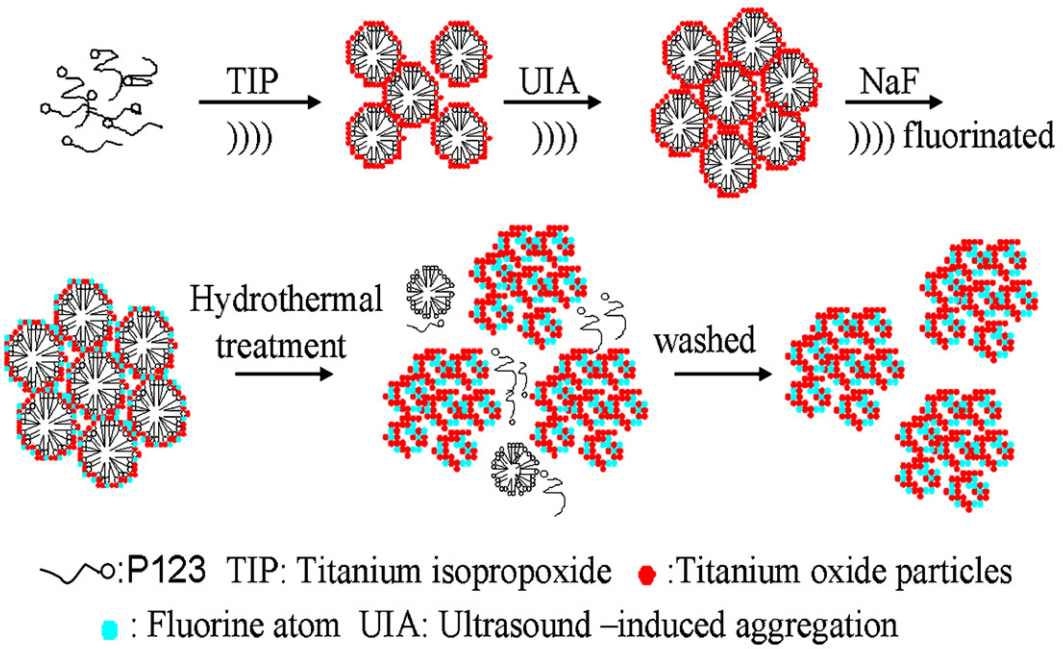

Fig. 8. Schematic illustration of the formation of fluorinated TiO_2 microspheres.

titania. At the same time the amphiphilic template molecule are released from the pore and form the mesostructured microspheres. Finally, the template is removed in washing process, as confirmed by the FT–IR measurements.

3.7. Activity test of the as-synthesized TiO_2 microspheres

The photocatalytic activity of the TiO_2 microspheres was tested by degradation of MB as a model reaction. Prior to irradiation, the dispersions were magnetically stirred in the dark for 40 min to achieve the adsorption/desorption equilibrium between TiO_2 and MB. Fig. 9 shows the behaviors of adsorption and catalytic reaction in MB solution. We can see that the pre-adsorption measurement showed that only about 0.7% of MB was adsorbed on as-synthesized pure TiO_2 microspheres. A significant improvement in the adsorption of MB (to 5%) was observed over the as-synthesized fluorinated TiO_2 microspheres. The MB conversion was less than 11% in 60 min over the as-synthesized pure TiO_2 microspheres. However, over the fluorinated TiO_2 microspheres, the MB conversion increased to 84% which was about 7.6 times of that of pure TiO_2 microspheres. After the calcination treatment, a slight increase in activity over both pure TiO_2 microspheres and fluorinated TiO_2 microspheres was observed. The high activity over the as-prepared samples could ascribe to the high crystallization and the removal of template.

Fluoride ion is known to replace the surface hydroxyl groups of TiO_2 with Ti–F species and significantly changes the photocatalytic reactivity of TiO_2. In our experiment, the fluorination had not brought about the substantial changes in the texture of TiO_2 microspheres, such as in BET surface areas, pore structure, and crystalline phase. Other reasons should be responsible for the great enhancing photocatalytic activity by fluorination. About photocatalytic mechanism, one controversy is about the role of direct electron transfer to the hole versus hydroxyl radical oxidation of the organics [44]. In the case of photocatalytic oxidation of MB, the photogenerated holes firstly react with surface hydroxyl groups or water molecule to form $HO^{\cdot}$

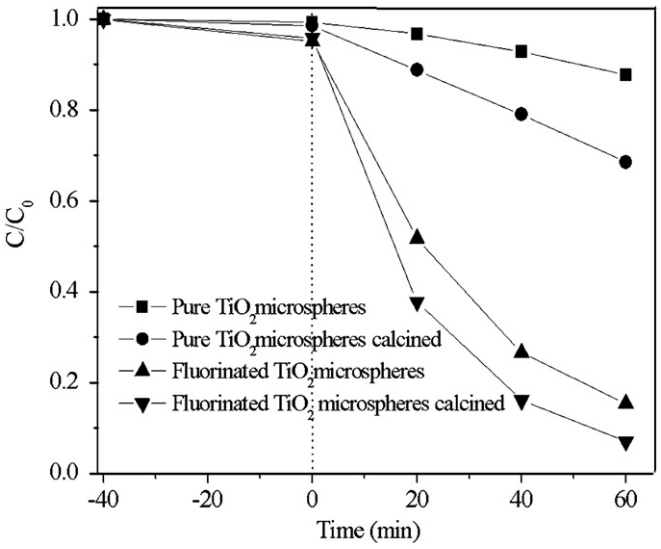

Fig. 9. Concentrations of methylene blue (MB) changes as a function of irradiation time in MB solution.

radicals, and the formed HO radicals subsequently oxidize MB molecules. In order to testify the reaction mechanism, *tert*-butyl alcohol was added to the MB solution. From Fig. 10, we can see that addition of 0.10 mol/L *tert*-butyl alcohol could significant inhibit the degradation of MB. This proved that the reaction is $HO^{\cdot}$ radical-mediated mechanism since alcohols could scavenge $HO^{\cdot}$ radicals effectively [45–47]. The rate constants were calculated according to pseudo-first-order model. The rate constant of fluorinated TiO_2 microspheres increased more than 13-fold (from $k = 0.13$ to $1.8\,h^{-1}$). But the inhibition of isopropanol is pronounced: the rate constants decreased to 0.10 and $1.18\,h^{-1}$ for pure and fluorinated TiO_2, respectively.

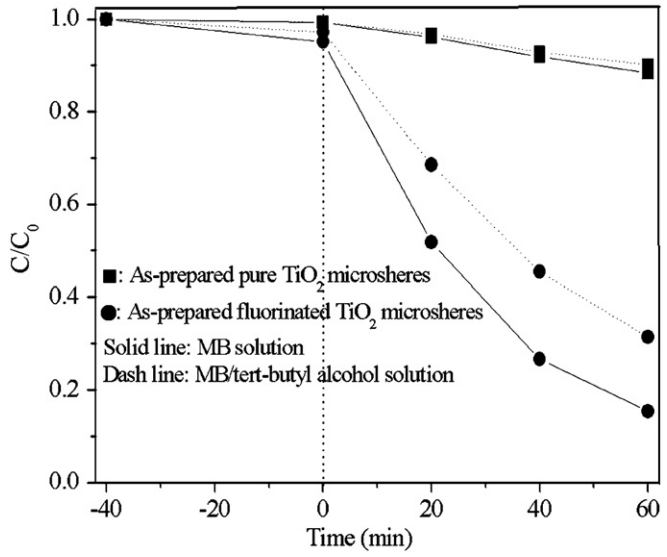

Fig. 10. Concentrations of methylene blue (MB) changes as a function of irradiation time in MB/tert-butyl alcohol solution.

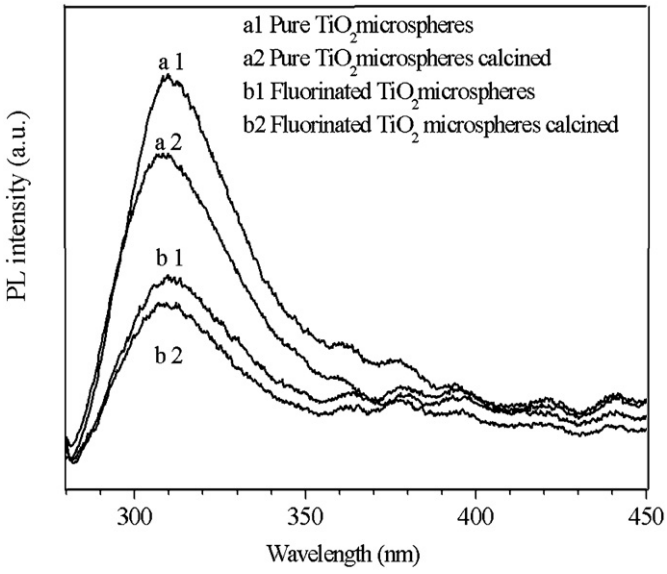

Fig. 11. The photoluminescence (PL) spectra of the samples.

As suggested by Yang [45], over fluorinated TiO_2 particles, more holes were available for producing more hydroxyl radicals. Simultaneously, the adsorption amount of MB near the surface was increased. As a result, the photocatalytic rate was enhanced by surface fluorination. Furthermore, the effects of fluorination on the recombination of photogenerated electron/hole pairs were measured by PL emission, as shown in Fig. 11.The intensity of the PL spectra for fluorinated TiO_2 samples is lower than that of pure TiO_2. Since the observed PL spectrum in TiO_2 can be attributed to the radiative recombination process of self-trapped excitations [48,49], or hydroxylated Ti^{3+} surface complexes [50] from the charge transfer excited state of the highly dispersed titanium oxide species. The reduction of PL intensity in the fluorinated TiO_2 indicates the decrease in the radiative recombination process. As a result, more holes were available for producing more hydroxyl radicals over the fluorinated TiO_2 sample.

4. Conclusions

A novel method for preparing highly photoactive fluorinated mesoporous TiO_2 microspheres was developed by a combined ultrasonic and hydrothermal treatment. Under ultrasound irradiation, an efficient fluorination reaction took place by a simple ligand exchange between surface hydroxyl groups on TiO_2 and fluoride ions. The hydrothermal treatment was effective for enhancing the crystallinity of the product and removing the P123 template. The high photocatalytic activity could be attributed to the abundance of hydroxyl radicals over the fluorinated mesoporous TiO_2 microspheres.

Acknowledgment

This work was supported by a Strategic Investments Scheme administrated by The Chinese University of Hong Kong.

References

[1] M. Gratzel, Nature 414 (2001) 338.
[2] M.A. Fox, M.T. Dulay, Chem. Rev. 93 (1993) 341.
[3] R. Wang, K. Hashimoto, A. Fujishima, M. Chikuni, E. Kojima, A. Kitamura, M. Shimohigoshi, T. Watanabe, Nature 388 (1997) 431.
[4] W.K. Ho, J.C. Yu, S.C. Lee, J. Solid State Chem. 179 (2006) 1171.
[5] J. Zhang, Q. Xu, Z.C. Feng, M.J. Li, C. Li, Angew. Chem. Int. Ed. 47 (2008) 1766.
[6] X.C. Wang, J.C. Yu, C.M. Ho, A.C. Mak, Chem. Commun. (2005) 2262.
[7] J.C. Yu, G.S. Li, X.C. Wang, X.L. Hu, C.W. Leung, Z.D. Zhang, Chem. Commun. (2006) 2717.
[8] J.C. Yu, L. Wu, J. Lin, P.S. Li, Q. Li, Chem. Commun. (2003) 1552.
[9] J.H. Park, S. Kim, A.J. Bard, Nanoletters 6 (2006) 24.
[10] X.C. Wang, J.C. Yu, Y.L. Chen, L. Wu, X.Z. Fu, Environ. Sci. Technol. 40 (2006) 2369.
[11] F.H. Tian, C.B. Liu, J. Phys. Chem. B 110 (2006) 17866.
[12] X.L. Yan, T. Ohno, K. Nishijima, R. Abe, B. Ohtani, Chem. Phys. Lett. 429 (2006) 606.
[13] J.C. Yu, J.G. Yu, W. Ho, Z. Jiang, L. Zhang, Chem. Mater. 14 (2002) 3808.
[14] C. Minero, G. Mariella, V. Maurino, E. Pelizzetti, Langmuir 16 (2000) 2632.
[15] M.S. Vohra, S. Kim, W. Choi, J. Photochem. Photobiol. A 160 (2003) 55.
[16] H. Park, W. Choi, J. Phys. Chem. B 108 (2004) 4086.
[17] J. Ryu, W. Choi, Environ. Sci. Technol. 38 (2004) 2928.
[18] J.S. Park, W. Choi, Chem. Lett. 34 (2005) 1630.
[19] H. Kim, W. Choi, Appl. Catal. B 69 (2007) 127.
[20] G.S. Wu, A.C. Chen, J. Photochem. Photobiol. A Chem. 195 (2008) 47.
[21] P.D. Yang, D.Y. Zhao, D.I. Margolese, B.F. Chmelka, G.D. Stucky, Chem. Mater. 11 (1999) 2813.
[22] P. Kluson, P. Kacer, T. Cajthaml, M. Kalaji, J. Mater. Chem. 11 (2000) 644.
[23] D.M. Antonelli, Micropor. Mesopor. Mater. 30 (1999) 315.
[24] P. Yang, D. Zhao, D.I. Margolese, B.F. Chmelka, G.D. Stucky, Lett. Nat. 396 (1998) 152.
[25] Y.K. Hwang, K.C. Lee, Y.U. Kwon, Chem. Commun. (2001) 1738.
[26] W. Yu-de, M. Chau-lai, S. Xiao-dan, L. Heng-de, Appl. Catal. A Gen. 246 (2003) 161.
[27] T. Alapi, P. Sipos, I. Ilisz, G. Wittmann, Z. Ambrus, I. Kiricsi, K. Mogyoro'si, A. Dombi, Appl. Catal. A Gen. 303 (2006) 1.
[28] K.S. Suslick, G.J. Price, Annu. Rev. Mater. Sci. 29 (1999) 295.
[29] J.C. Yu, L.Z. Zhang, J.G. Yu, New J. Chem. 26 (2002) 416.
[30] J.C. Yu, X.C. Wang, L. Wu, W.K. Ho, L.Z. Zhang, G.T. Zhou, Adv. Funct. Mater. 14 (2004) 1178.
[31] Y. Koltypin, S.I. Nikitenko, A. Gedanken, J. Mater. Chem. 12 (2002) 1107.
[32] K. Okitsu, Y. Mizukoshi, H. Bandow, Y. Maeda, T. Yamamoto, Y. Nagata, Ultrason. Sonochem. 3 (1996) 249.
[33] T. Hyeon, M. Fang, K.S. Suslick, J. Am. Chem. Soc. 118 (1996) 5492.
[34] J.J. Zhu, S.T. Aruna, Yu. Koltypin, A. Gedanken, Chem. Mater. 12 (2000) 143.
[35] M.M. Mdleleni, T. Hyeon, K.S. Suslick, J. Am. Chem. Soc. 120 (1999) 6189.
[36] L.Z. Zhang, J.C. Yu, Chem. Commun. (2003) 2078.
[37] J.C. Yu, J.G. Yu, L.Z. Zhang, W.K. Ho, J. Photochem. Photobiol. A Chem. 148 (2002) 263.
[38] H. Zhang, J.F. Banfield, J. Phys. Chem. B 104 (2000) 3481.
[39] Y.L. Su, X.W. Zhang, M.H. Zhou, S. Han, L.C. Lei, J. Photochem. Photobiol. A Chem. 194 (2008) 152.
[40] D. Li, H. Haneda, S. Hishita, N. Ohashi, N.K. Labhsetwar, J. Fluorine Chem. 126 (2005) 69.
[41] D. Li, N. Ohashi, S. Hishita, T. Kolodiazhnyi, H. Haneda, J. Solid State Chem. 178 (2005) 3293.
[42] D.G. Shchukin, D.V. Sviridov, J. Photochem. Photobiol. C Photochem. Rev. 7 (2006) 23.
[43] S. Ramesh, Y. Koltypin, A. Gedanken, J. Mater. Sci. 12 (1997) 3271.
[44] D. Hufschmidt, L. Liu, V. Seizer, Water Sci. Technol. 49 (4) (2004) 135.

[45] S.Y. Yang, Y.Y. Chen, J.G. Zheng, Y.J. Cui, J. Environ. Sci. 19 (2007) 8689.
[46] C. Richard, F. Bosquet, J.F. Pilichowski, J. Photochem. Photobiol. A Chem. 108 (1) (1997) 45.
[47] C. Minero, G. Mariella, V. Maurino, D. Vione, E. Pelizzetti, Langmuir 16 (2000) 8964.
[48] C. Yang, M. Wohlgenannt, Z.V. Vardeny, W.J. Blau, A.B. Dalton, R. Baughman, A.A. Zakhidov, Physica B 338 (2003) 366.
[49] Y. Yu, J.C. Yu, J.G. Yu, Y.C. Kwok, Y.K. Che, J.C. Zhao, L. Ding, W.K. Ge, P.K. Wong, Appl. Catal. A 289 (2005) 186.
[50] M. Anpo, N. Alkawan, Y. Kubokaway, J. Phys. Chem. 89 (23) (1985) 5017.